

Growth of C-S-H phases on different metallic surfaces

Maximilian Schleiting¹  | Alexander Wetzel¹  | Daniela Göbel¹ |
Philipp Krooß² | Johanna-Maria Frenck² | Thomas Niendorf² |
Bernhard Middendorf¹

¹Department of Structural Materials and Construction Chemistry, University of Kassel, Kassel, Germany

²Institute of Material Engineering, University of Kassel, Kassel, Germany

Correspondence

Maximilian Schleiting, Department of Structural Materials and Construction Chemistry, University of Kassel, 34125 Kassel, Germany.

Email: schleiting@uni-kassel.de

Abstract

The influence of reinforcement, especially fibre reinforcement in ultra-high performance concrete is strongly dependent on the bonding (adhesive, shear and friction bond) between metallic surface and cementitious matrix. As usually straight fibres are used for fibre reinforcement and, thus, no significant mechanical bonding is existent, the adhesive bond is particularly important. Previous studies stated that the adhesive bonding behaviour between metallic materials and cementitious matrix strongly depends on the chemical composition of metallic alloys. Therefore, in order to address this topic, the present study investigates the growth of C-S-H phases on stainless steel and on cold drawn steel. This growth process was realised by a surface treatment of the metallic alloys using a synthetically manufactured Tricalciumsilicate (C_3S) powder diluted in water. After defined times of the C_3S treatment the process is stopped to get a time dependent growing behaviour of the cementitious phases. Light microscopy as well as scanning electron microscopy was used in order to investigate the surfaces following the application of the C_3S . The results reveal that the growth of C-S-H phases is more dependent on the metallic surface and its topography than on the alloy composition.

KEYWORDS

fibre/matrix bond, microstructure, reinforcement, ultra-high performance concrete

1 | INTRODUCTION

Ultra-high performance concrete (UHPC) is characterised by a very dense structure gained by a high packing density of the fines like cement, silica fume and quartz powder, a low water/cement ratio of about 0.20–0.25 and, therefore, the use of superplasticisers, leading to a high compressive strength of above 150 N/mm².¹ Accompany-

ing with these superior material properties, the failure behaviour of UHPC can be described as explosive due to the dense matrix.^{2–4} To improve mechanical characteristics under tensile forces and counteract the explosive failure behaviour (micro-) fibre reinforcement is used with a fibre content of about 1–2 vol%.^{5,6} Mostly, metallic fibres are used in concretes, as these are widely available and have enhanced mechanical properties. The effectiveness of

This is an open access article under the terms of the [Creative Commons Attribution-NonCommercial-NoDerivs](https://creativecommons.org/licenses/by-nc-nd/4.0/) License, which permits use and distribution in any medium, provided the original work is properly cited, the use is non-commercial and no modifications or adaptations are made.

© 2022 The Authors. *Journal of Microscopy* published by John Wiley & Sons Ltd on behalf of Royal Microscopical Society

TABLE 1 Overview of the test setups

Sample	Treatment	C ₃ S solution					
		1:150	1:300	1:400	1:500	1:1000	1:1800
SS	–	x	x	x			
CD	–	x	x	x			
F_CD	Annealed			x	x	x	x

the fibre reinforcement is strongly dependent on the bonding (adhesive, shear and friction bond) between metallic surface and cementitious matrix. In case of straight fibres, where no significant mechanical bonding is existent, the adhesive bond is particularly important.^{7,8} The interfacial transition zone is strengthened in UHPC as the use of silica fume leads to an increased amount of Calcium-Silicate-Hydrate (C-S-H) phases in the zone due to the secondary reaction from Calcium Hydroxide and, therefore, improves the adhesive bond between fibre and matrix. However, previous studies indicated a varying efficiency of different metallic fibre materials.^{9,10} This was quantified by fibre pullout tests. The results revealed that the bond stress could vary significantly as a function of the alloy composition as well as of coatings of the fibre. In order to investigate these differences in the bond strength between different metallic fibres and the cementitious UHPC matrix, this study examines the microstructural growth of C-S-H phases on different metallic surfaces in view of the C₃S saturation, sample topography and the composition of the metal alloy as well as metallic microstructure.

2 | MATERIAL AND METHODS

For the metallic material different alloys were investigated. For the tests, flat specimen (5 × 20 mm) of X5CrNi18-10 stainless steel (SS) and 100MnCrW4 cold drawn work steel (CD) were used. The latter material revealed corrosion before the first tests; therefore, polished fibres of the cold drawn steel material (F_CD) were used. The fibres were heated up to 900°C for 30 min to promote larger metal crystallites in order to analyse them with electron backscatter diffraction (EBSD) measurements. This is contrary to a realistic fibre microstructure but was chosen as a model system to increase a possible influence of crystallite boundaries and orientation.

For the growth of C-S-H phases, synthetically manufactured Tricalciumsilicate (C₃S) powder in different concentrations diluted in distilled water was used. The concentrations were in a range of 1:150 (1 part C₃S, 150 parts water) to 1:1800 by mass (Table 1). The specimen were then dipped into the solution for different time periods (5 min up to 2 days) to get time resolved information about the growth process of the C-S-H phases. This pro-

cess was carried out in a glovebox flooded with nitrogen to minimise contamination with air and dust. Afterwards, optical investigations of the specimen were done with an environmental scanning electron microscope (ESEM) in low- and high-vacuum mode using secondary electron (SE) and backscattered electron (BSE) images. Prior to the immersion tests, some of the specimen were analysed with electron backscattered diffraction (EBSD) measurements to allow a correlation between the crystallographic orientations and the grain boundary character with the growth process of the C-S-H phases. Therefore, the investigated specimen were ground down to 5 µm grit size and vibration-polished for 2 h using a colloidal SiO₂ suspension with 0.02 µm particle. EBSD measurements were then performed using a scanning electron microscope operated at 20 kV.

Additionally, fibre pullout tests with regular and annealed cold drawn fibres (F_CD) were carried out on five specimen for both fibre types. For the tests, fibre rows of five fibres were pulled out of a UHPC matrix, revealing an average maximum pullout force, which can be translated to a maximum bond stress using the following formula:

$$\tau_{\max} = \frac{F_{\max}}{d_f \times \pi \times l_e}, \quad (1)$$

where F_{\max} is the average maximum pullout load, d_f is the fibre diameter and l_e is the embedded fibre length.^{9,10}

3 | RESULTS

Applying the flat stainless steel (SS) and cold drawn (CD) samples in an oversaturated aquatic C₃S solution (ratio of 1:150) revealed that already after 10 min first C-S-H seeds were formed and after 25 min larger parts of the specimen were overgrown by C-S-H phases, forming ‘C-S-H isles’ (SS sample exemplary in Figure 1A). These phases often grow on dark isle structures that formed prior to the C-S-H phases. In addition, on the samples that were exposed to the oversaturated solution, often CaOH₂ crystals were found (Figure 1A). Lowering the concentration of the C₃S to a ratio of 1:400 leads to a much lower abundance of C-S-H seeds on the surface. After 20 min, only single crystals were visible and no connected parts as in case of the

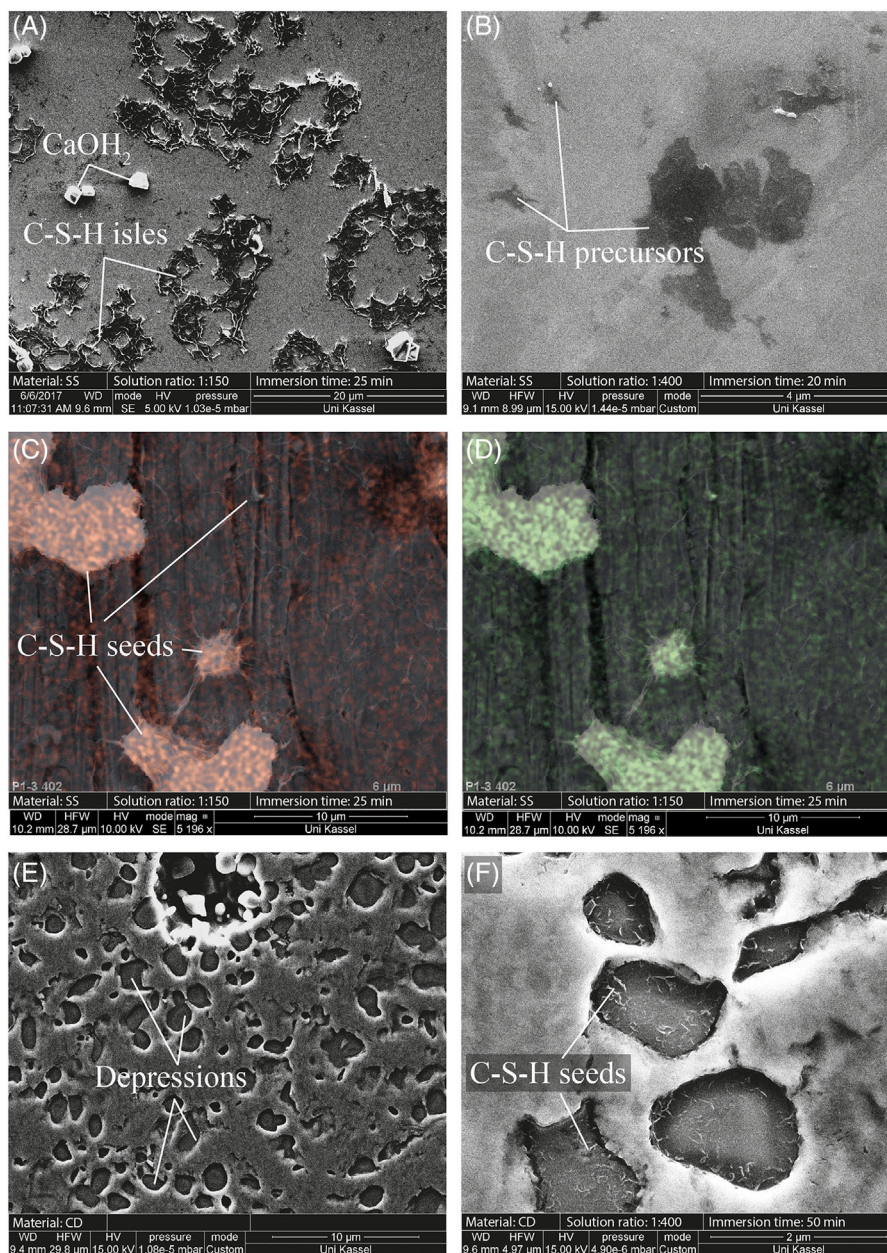


FIGURE 1 (A) SS sample after 25 min in an oversaturated C_3S solution (1:150). Large parts of the specimen are covered with C-S-H phases. Dark isles serve as crystallisation seeds for the C-S-H phases. In the oversaturated solution, $CaOH_2$ crystals can be seen. (B) Stainless steel after 20 min in a C_3S solution with a ratio of 1:400. Only single C-S-H seeds are visible. (C) SS fibre after 25 min in a C_3S solution with a ratio of 1:150. Overlaid is a transparent EDX mapping of calcium, identifying the phases as C-S-H phases / C-S-H seeds (in combination with Figure 1D). (D) SS fibre after 25 min in a C_3S solution with a ratio of 1:150. Overlaid is a transparent EDX mapping of silicon, identifying the phases as C-S-H phases/C-S-H seeds (in combination with Figure 1C). (E) General topography of the corroded CD specimen. (F) CD sample after 50 min in the C_3S solution with a ratio of 1:400. First C-S-H phases formed within the depressions of the sample. Mostly single crystals are visible. No isles formed. All images in SE or custom (mixture of SE and BSE) mode. Figure 1C and D with overlaying EDX mapping

oversaturated solution were found. After 30 min in the same solution, the number of C-S-H seeds increased and some smaller C-S-H isles (or their precursors that could be calcite based or due to corrosion effects) were visible (Figure 1B). Figure 1C and D shows C-S-H phases exemplary on non-polished fibres. Selective EDX measurements and EDX mappings [Ca (red) in Figure 1C and Si (green)

in Figure 1D] clearly shows an accumulation of silicon and calcium on the isle-like structures, identifying these as C-S-H phases/C-S-H seeds.

In case of the flat cold drawn steel (CD), the general appearance and topography of the sample look very different (Figure 1E). Clearly visible depressions due to corrosion are spread over the whole sample and a topographic

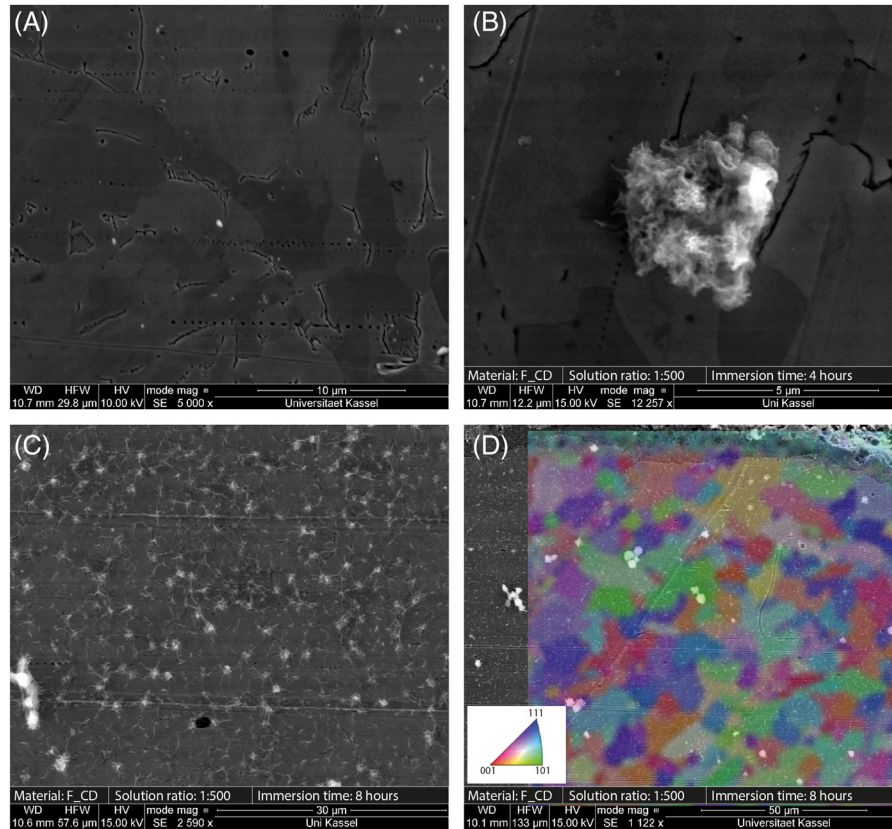


FIGURE 2 (A) Overview of the polished fibre surface. (B) Single C-S-H isle connected to gap in the fibre after 4 h in a 1:500 C_3S solution. (C) Fine coating of C-S-H phases on the polished fibre after 8 h in a 1:500 C_3S solution. (D) SE image with overlapped transparent EBSD measurement of the polished fibre after 8 h in a 1:500 C_3S solution. The overlapped image displays the EBSD inverse pole figure (IPF) map of the ferrite phase. The IPF map was plotted with respect to the normal direction. The corresponding color-coded standard triangle is shown in D. Larger C-S-H isles are found mostly at or near grain boundaries. All images in SE mode

effect was expected. In general, the crystallisation process at the surface began later compared to the stainless steel sample. With a concentration of 1:400, the first C-S-H phases were found about 50 min after exposing the specimen to the C_3S solution (Figure 1F). The first crystals formed within the depressions of the steel sample.

The fibre specimen (F_CD) showed similar results as the cold drawn flat samples. The untreated (not exposed to the C_3S solution) sample (Figure 2A) revealed more topographic patterns than the flat stainless steel specimen, however, not as distinct as in the CD specimen. To achieve a slower growing process and, therefore, a finer and more specific growing pattern, the sample was exposed to a C_3S solution with a ratio of 1:1800. However, no C-S-H phases were found following 2 days of exposure. Therefore, the concentration of C_3S was evenly increased up to a ratio of 1:500. On the sample in this solution, isolated C-S-H isles were found first after 4 h. These formed mainly along grain boundaries of the sample, however, have also overgrown flat areas of the sample (Figure 2B). After 8 h in the same solution, the whole sample was overgrown by fine C-S-H phases (Figure 2C). Also large C-S-H isles are exist-

ent. EBSD measurements of both, flat (not shown here) and polished fibre specimen (Figure 2D), revealed that a growth of C-S-H phases does not correlate with the orientation of the metal grains, however, it was confirmed that larger C-S-H phases are preferentially growing at crystallite boundaries (Figure 2D).

Fibre pullout tests of regular and annealed fibres (F_CD) out of a UHPC matrix revealed no significant differences in the bond strength as well as in post failure behaviour. Regular and annealed fibres had a bond strength of 4.21 MPa (± 0.49 MPa) and 4.26 MPa (± 0.57 MPa), respectively (Figure 3).

4 | SUMMARY AND DISCUSSION

The results have shown that the growth of C-S-H phases on metallic surfaces based on a C_3S solution correlates with different parameters. First of all the concentration of the C_3S influences the growing speed of the C-S-H phases.¹¹ In an oversaturated solution, the very first phases are formed within a few minutes, while in solutions with lower

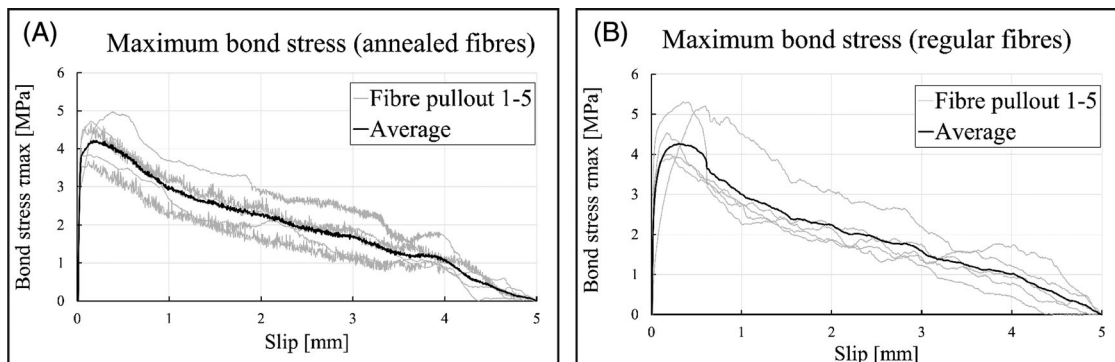


FIGURE 3 Results of the fibre pullout tests for cold drawn steel fibres (F_CD). (A) Specimen with annealed fibres: bond stress – slip relation of the five specimen (grey lines) and average (black graph). (B) Specimen with regular fibres: bond stress – slip relation of the five specimen (grey lines) and average (black graph)

concentrations (1:500 and lower) hours up to days are needed in order to form the first C-S-H phases.

Stainless steel in a highly concentrated solution (1:400 and higher) revealed a specific growing pattern. In the first minutes, dark isles were formed, serving as a seed area for C-S-H phases. Within a few minutes, the C-S-H phases began to grow on these isles (Figure 1A, C and D). This growing pattern can be described after Vollmer-Weber (Isle-like growth).¹² Furthermore, much more $\text{Ca}(\text{OH})_2$ crystals were found at the surface of the specimen in the oversaturated solution compared to the lower concentrated solutions. In the latter, C-S-H phases often occur as single crystals. Connected C-S-H phases are not visible within the first 50 min; just some small precursor areas were found (Figure 1B). This behaviour could be described after Frank-van-der-Merwe.¹² In this case, single crystals form separate layers that are later overgrown by the next layer, repeating this process up to a full coverage of the surface.

Another important influence on the growing behaviour of the C-S-H phases is the topography of the samples. In case of the cold drawn steel, single C-S-H crystals began to grow within depressions on the sample. In case of the fibre sample (F_CD), the first single C-S-H phases as well as small C-S-H isles were found always connected to grain boundaries. Therefore, it is likely that these topographic features (depressions and grain boundaries) favour the growth of C-S-H phases. However, at a longer exposure to the C_3S solution, an evenly coating of the fibre with C-S-H phases was found regardless of topographic features on the sample. Furthermore, the fibre pullout tests of annealed and regular fibres (F_CD) revealed no significant differences in bond stress between fibre and cementitious matrix.

In case of alloy composition of the fibre material, no final conclusion can be drawn here. As the topography of the alloys significantly differs, no clear conclusion can be


drawn, whether the differences of the growing behaviour stems also from the alloy composition. Both cold drawn specimen (CD and F_CD) had topographic impurities on the sample and in both cases, these depressions served as preferred growing spot for C-S-H phases. In contrast, on flat areas of both samples, only a few single C-S-H phases and C-S-H isles were found in case of short exposure times (<4 h). Only after longer exposure times (8 h), a fine coating of C-S-H phases was found all over the fibre sample.

ACKNOWLEDGMENTS

Open access funding enabled and organized by Projekt DEAL.

ORCID

Maximilian Schleiting  <https://orcid.org/0000-0003-2555-7510>

Alexander Wetzel  <https://orcid.org/0000-0003-2680-9708>

REFERENCES

- Bornemann, R., Schmidt, M., Fehling, E., & Middendorf, B. (2001). Ultra-Hochleistungsbeton UHPC—Herstellung, Eigenschaften und Anwendungsmöglichkeiten. *Beton- und Stahlbetonbau*, 96, 458–467. <https://doi.org/10.1002/best.200100550>.
- Kusumawardaningsih, Y., Fehling, E., Ismail, M., & Aboubakr, A. A. M. (2015). Tensile strength behavior of UHPC and UHPFRC. *Procedia Engineering*, 125, 1081–1086. <https://doi.org/10.1016/j.proeng.2015.11.166>.
- Shi, C., Wu, Z., Xiao, J., Wang, D., Huang, Z., & Fang, Z. (2015). A review on ultra high performance concrete: Part I. Raw materials and mixture design. *Construction and Building Materials*, 101, 741–751. <https://doi.org/10.1016/j.conbuildmat.2015.10.088>.
- Wang, D., Shi, C., Wu, Z., Xiao, J., Huang, Z., & Fang, Z. (2015). A review on ultra high performance concrete: Part II. Hydration, microstructure and properties. *Construction and Building Materials*, 96, 368–377. <https://doi.org/10.1016/j.conbuildmat.2015.08.095>.

5. Wietek, B. (2010). *Stahlfaserbeton*. Springer Fachmedien, ISBN 9783834808721.
6. Leutbecher, T., & Fehling, E. (2012). Tensile behavior of ultra-high-performance concrete reinforced with reinforcing bars and fibers: Minimizing fiber content. *ACI Structural Journal*, 109, <https://doi.org/10.14359/51683636>.
7. Gutowski, W. (1990). Effect of fibre-matrix adhesion on mechanical properties of composites. In H. Ishida (Ed.), *Controlled interphases in composite materials* (pp. 505–520). Springer Netherlands: Dordrecht, ISBN 978-94-011-7818-1.
8. Parker, B. M. (1994). Adhesive bonding of fibre-reinforced composites. *International Journal of Adhesion and Adhesives*, 14, 137–143. [https://doi.org/10.1016/0143-7496\(94\)90009-4](https://doi.org/10.1016/0143-7496(94)90009-4).
9. Schleiting, M., Wetzel, A., Krooß, P., Thiemicke, J., Niendorf, T., Middendorf, B., & Fehling, E. (2020). Functional microfibre reinforced ultra-high performance concrete (FMF-UHPC). *Cement and Concrete Research*, 130, 105993, <https://doi.org/10.1016/j.cemconres.2020.105993>.
10. Wiemer, N., Wetzel, A., Schleiting, M., Krooß, P., Vollmer, M., Niendorf, T., Böhm, S., & Middendorf, B. (2020). Effect of fibre material and fibre roughness on the pullout behaviour of metallic micro fibres embedded in UHPC. *Materials (Basel)*, 13, 3128, <https://doi.org/10.3390/ma13143128>.
11. Bellmann, F., & Scherer, G. W. (2018). Analysis of C-S-H growth rates in supersaturated conditions. *Cement and Concrete Research*, 103, 236–244. <https://doi.org/10.1016/j.cemconres.2017.05.007>.
12. Oppen, G., Busch, M., & Lüders, K. (2015). *Quantenphysik: Atomare Teilchen und Festkörper*, 1. Aufl.; Walter de Gruyter GmbH Co.KG: s.l. ISBN 3110226715.

How to cite this article: Schleiting, M., Wetzel, A., Göbel, D., Krooß, P., Frenck, J.-M., Niendorf, T., & Middendorf, B. (2022). Growth of C-S-H phases on different metallic surfaces. *Journal of Microscopy*, 286, 148–153. <https://doi.org/10.1111/jmi.13089>